Theoretical study of structural, electronic, and magnetic properties of Au_nM^+ clusters (M=Sc, Ti, V, Cr, Mn, Fe, Au; $n \leqslant 9$)

M. B. Torres*
Departamento de Matemáticas y Computación, Universidad de Burgos, 09006 Burgos, Spain

E. M. Fernández† and L. C. Balbás‡
Departamento de Física Teórica, Universidad de Valladolid, E-47011 Valladolid, Spain
(Received 19 November 2004; published 21 April 2005)

We investigate the element- and size-dependent electron stability of Au_nM^+ clusters (M=Sc, Ti, V, Cr, Mn, Fe, Au; $n \leqslant 9$) by means of first-principles density functional calculations. The interplay between the cluster atomic arrangements and their electronic and magnetic structure is studied for the few lowest energy isomeric states and their dependence on the dopant atom and its environment in the host cluster. Our total energy calculations provide a clear explanation of the abundance peaks observed recently in photofragmentation experiments. The magnetic and geometrical configurations are strongly correlated. The local magnetic moment of the dopant atom shows a pronounced odd-even oscillation with the number of Au atoms, and decreases when the cluster size increases.

DOI: 10.1103/PhysRevB.71.155412 PACS number(s): 73.22.−f, 36.40.Cg, 36.40.Qv, 71.15.Mb

I. INTRODUCTION

The influence of transition metal (M) impurities on the electric transport in gold nanocontacts[1] is an example, among many others, of interesting items in the study of gold clusters doped with transition metal atoms. Recent experimental[2–6] and theoretical work[3,7–11] has demonstrated that the introduction of a dopant atom in a metal cluster can change its structure and electromagnetic properties significantly.

Neukermans and co-workers[2] have investigated the stability of cationic clusters Au_nM^+, with M from Sc to Ni, by means of photofragmentation experiments. The observed intensity, I_n, shows an enhanced abundance for specific cluster sizes, corresponding to Au_nM^+ clusters with favored stability (magic numbers).[12] In the range $n \leqslant 9$, these magic numbers n are 6 (Sc), 5 (Ti), 5 and 7 (V, Cr, Mn, Fe, Co), 2 and 8 (Ni), and 3 and 9 (Au). A qualitative explanation of these magic numbers was given[2] in terms of a phenomenological shell model, which leads to magic numbers for electronic shell closing with 2, 8,…, electrons. Thus, in addition to 1 delocalized 6s electron for each Au atom, one need to assume two 4s delocalized electrons for all the transition metal elements from Sc to Co, plus one (Sc), two (Ti), or zero (V to Co) 3d delocalized electrons. For Ni, with a $3d^8 4s^2$ atomic configuration, only 1 valence electron is required to explain the observed magic numbers within the shell model. That means that the 3d electrons are completely delocalized in Sc and Ti, and completely localized in the remaining 3d M series. To justify that Cr and Ni dopants act as divalent and monovalent metals, respectively, in a Au matrix, a small promotion energy between configurations $3d^x s^2$ and $3d^{x+1}s^1$ was invoked.[2] A more quantitative study of the delocalization trends of d electrons, based in density functional theory (DFT), has been performed recently[3] for Au_5M^+ (M=Sc, Ti, Cr, Fe, Au). In this paper we present spin-density functional calculations for a wider range of 3d dopant atom and cluster sizes, aimed at explaining the experimental magic numbers, bonding properties, and local magnetic moments from a first principles approach.

The intensity, I_n, of Au_nM^+ clusters resulting from a unimolecular fragmentation experiment[2] can be related to the Helmholtz free energy at temperature T, $F_n(T)$, by[12]

$$\ln(I_n/I_{n+1}) = \Delta_2 F_n(T)/k_B T, \tag{1}$$

where $\Delta_2 F_n$ is the second difference in Helmholtz free energy. In the asymptotic limit of zero temperature, the rhs of Eq. (1) is approximated by the second difference of total energy, E_n, of the Au_nM^+ cluster,

$$\Delta_2 E_n = E_{n+1} + E_{n-1} - 2E_n \tag{2}$$

$$= E_{ev}(n) - E_{ev}(n+1), \tag{3}$$

where $E_{ev}(n) = E_{n-1} + E_{\mathrm{Au}} - E_n$ is the monomer evaporation energy needed for the process in which Au_nM^+ loses Au atoms, with energy E_{Au}, one by one. We see in Eq. (3) that positive values of $\Delta_2 E_n$ indicate that Au_nM^+ is more stable to the evaporation of an Au atom than $Au_{n+1}M^+$. Negative values of $\Delta_2 E_n$ correspond to experimental abundances $I_n < I_{n+1}$, according to Eq. (1).

In this paper we investigate the correspondence of the magic numbers observed in the abundance spectra of photofragmented Au_nM^+ clusters, with the enhanced peaks of $\Delta_2 E_n$ calculated from first principles. Details of the calculations are given in Sec. II. In Sec. III we present and discuss our results. The equilibrium geometries, binding energies, and the spin multiplicity of the few lowest energy isomeric states of Au_nM^+ clusters are discussed in Sec. III A. The trends of the local charge and magnetic moment of the impurity atom are discussed in Sec. III B. In Sec. IV we present the conclusions.

II. COMPUTATIONAL PROCEDURE

We use the first-principles code SIESTA[13] to solve fully self-consistently the standard Kohn-Sham equations[14] of density-functional theory (DFT) within the spin-polarized

 ©2005 The American Physical Society

generalized-gradients functional aproximation (GGA) for the exchange-correlation potential as parametrized by Perdew, Burke, and Ernzerhof.[15] We use norm conserving scalar relativistic pseudopotentials[16] in their fully nonlocal form,[17] generated from the atomic valence configurations $5d^{10}6s^16p^0$ for Au, and $4s^23p^63d^q$ for the M elements ($q=1$, 2, 3, 4, 5, 6 for Sc, Ti, V, Cr, Mn, Fe, respectively), and core radii which we have tested and reported in previous works.[18,19] We have included in the valence the semicore orbital $5d$ in Au, and $3p$ in M elements. Specifically, for $4s$, $3p$, $3d$ orbitals we use the core radii, in a.u., 2.57, 1.08, 1.38 (Sc, Ti, V), 2.36, 1.09, 1.09 (Cr), 2.47, 1.29, 1.29 (Mn), and 2.47, 1.00, 1.00 (Fe). Flexible linear combinations of numerical (pseudo) atomic orbitals are used as the basis set, allowing for multiple-ζ and polarization orbitals. In order to limit the range of the basis pseudoatomic orbitals (PAO), they are slightly excited by a common "energy shift" (0.05 eV in this work), and truncated at the resulting radial node. In the present calculations we used, for M elements, double-ζ $3p$, $4s$, $3d$-basis and single $4p$ polarization orbital, with maximum cutoff radii, in Bohr, 9.07 (Sc), 8.66 (Ti), 8.49 (V), 8.35 (Cr), 8.01 (Mn), and 7.90 (Fe). For Au we used a double-ζ $5d$, $6s$-basis, with maximum cutoff radius 7.62 Bohr. The basis functions and the electron density are projected onto a uniform real space grid in order to calculate the Hartree and exchange-correlation potentials and matrix elements. The grid fineness is controlled by the "energy cutoff" of the plane waves that can be represented in it without aliasing (100 Ry in this work). Convergence tests with respect to size and cutoff radii of basis sets, and with respect to LDA or GGA xc functionals, were presented in previous works.[18,19]

To obtain the equilibrium geometries, an uncostrained conjugate-gradient structural relaxation using the DFT forces[20] was performed for several initial cluster structures (typically more than ten), suggested by the isomeric geometries for Au_n, Au_n^-, and Au_n^+ clusters obtained previously.[18]

III. RESULTS AND DISCUSSIONS

A. Equilibrium geometries, spin multiplicity, and binding energy

In Fig. 1 are shown the calculated equilibrium geometries of the few lowest energy isomers of cationic Au_nM^+ clusters with $2 \leqslant n \leqslant 9$ and M=Au, Sc, Ti, V, Cr, Mn, Fe. In Table I are given the average M-Au bond length, d_{av}, and the binding energy per atom,

$$E_b(\mathrm{Au}_nM^+) = \frac{nE_{\mathrm{Au}} + E_{M^+} - E_n}{n+1}. \tag{4}$$

The integrated difference of majority and minority spin electronic charges, denoted by M_z, is also given. Assuming that the cluster has M_z unpaired electrons, each one with spin $\frac{1}{2}$ (in units of $\hbar$), the multiplicity of the state is $M=M_z+1$, and the z component of magnetic moment due to spin is $\mu=M_z$ (in Bohr magnetons, μ_B).

The calculated M_z value of the lowest energy isomer of the Au_nM^+ cations is given in bold characters in Table I. For odd (even) n, M_z follows the sequence 1, 1, 2, 3, 4, 5, 4 (0, 0, 1, 4, 5, 4, 3) for M=Au, Sc, Ti, V, Cr, Mn, Fe, respectively, with the exceptions Au_9Ti^+, Au_9Mn^+, Au_9Fe^+, and Au_8V^+. For the three Au_9M^+ exceptions we find isomers with a slightly enlarged Au-M distance ($\sim$0.02 Å) and a slightly smaller binding energy ($\sim$0.02 eV/atom), which follow the general M_z sequence. These small differences mark the limit of our accuracy in the calculated bond distance and binding energy. For Au_8V^+, we find an isomer with 0.08 eV/atom higher energy which has $M_z=4$ (fulfilling the general M_z sequence) and the 2D geometry 8-II of Fig. 1. This planar geometry resembles an Au(111) surface with the M atom substituting for an Au atom, but having a smaller average M-Au distance than Au—Au atoms in the (111) surface. This interplay between spin multiplicity and the geometrical environment in Au_8M^+ is even more sensitive for M=Cr, Fe. We will comment below that interplay for Au_2M^+ clusters, as well as for Au_nM^+ clusters, will lead to general empirical rules.

Our multiplicities M_z+1 for Au_5M^+ coincide with the ones previously reported[3] for M=Sc, Ti, Cr, and disagree for Fe (we obtain 5 instead of 3). Considering the lowest energy isomer, the difference $M_z(n=\mathrm{odd})-M_z(n=\mathrm{even})$ is 1 for M=Au, Sc, Ti, Mn, Fe, and −1 for M=V, Cr. The difference in d occupations for up and down bands of M impurities in bulk Au, calculated recently by Frota-Pessôa[21] are 2.15 (V), 3.61 (Cr), 4.00 (Mn), and 2.95 (Fe), which are near to the lower of our calculated M_z values for the ground state of Au_nM^+ clusters with odd n (V, Cr), and even n (Mn, Fe).

As a general trend, we obtain planar geometries for the lowest energy isomer of clusters with $n \leqslant 6$, and three dimensional (3D) geometries for clusters with $n \geqslant 7$. The exceptions are Au_6Cr^+, which is 3D, and Au_8Sc^+ and Au_8Ti^+, which are planar (2D). In fact, we find a 2D isomer of Au_6Cr^+ with practically the same binding energy, but a smaller average M-Au bond distance, whereas for Au_8Sc^+ and Au_8Ti^+, we find 3D isomers with binding energy close to the planar ones, but with a larger average M-Au bond distance. In a sense, we can say that $n=7$ marks the onset of 3D geometries for Au_nM^+ clusters. For the second lowest energy isomer of clusters with $n \geqslant 3$ we obtain mostly 3D geometries. The exceptions are Au_8M^+ clusters with M=V, Cr, Mn, Fe, which have, however, a 3D ground state. Other exceptions are Au_4Mn^+, Au_5Sc^+, and Au_6Ti^+, whose first and second isomers are both planar.

The geometry of Au_2M^+ cations in the lowest energy state is an equilateral triangle (2-III in Fig. 1), except for M=Sc, Ti, which prefer an obtuse triangle with the M at the apex (2-I in Fig. 1). This tendency is reversed for the second isomer, which adopts the 2-I geometry for M=V, Mn, Fe, and the 2-III geometry, for M=Sc, Ti. For the second isomer of Au_2Cr^+ we find the obtuse triangle 2-II, with the M atom coordinated to only one Au. This configuration is less bonded by far than the lowest energy state 2-III, but still has larger binding energy than the isomer 2-I.

The average M-Au bond distance, d_{av}, of Au_2M^+ clusters is smaller for the obtuse triangle 2-I than for the equilateral triangle 2-III, except for Au_2Mn^+, where d_{av} is the same for both configurations. For Au_2Cr^+, d_{av} in the obtuse triangle 2-II is slightly larger than in the equilateral triangle 2-III geometry. This empirical relation between the average M

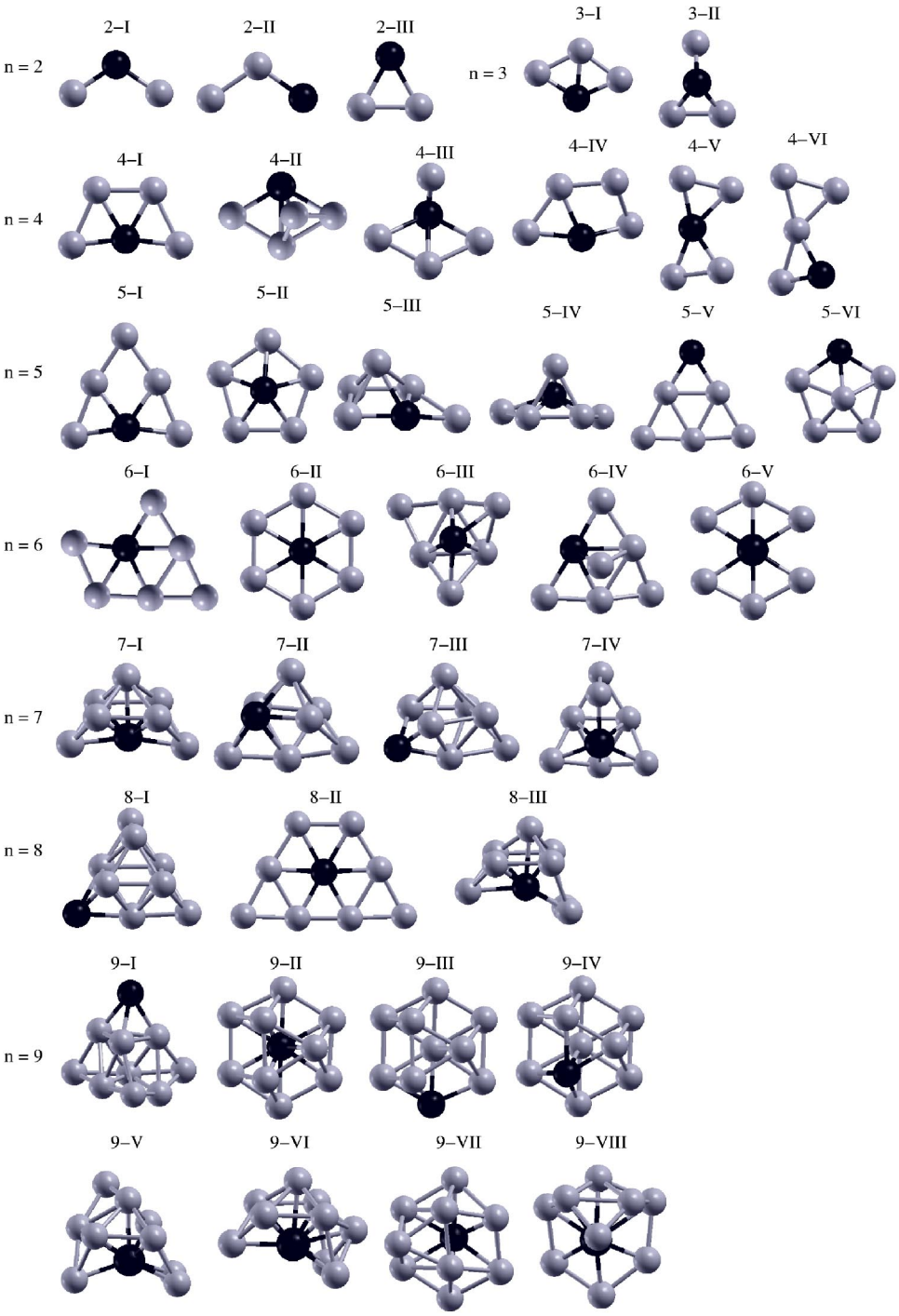

FIG. 1. Equilibrium geometries of the few lowest energy isomers of cationic Au_nM^+ clusters, with $2 \leqslant n \leqslant 9$ and M=Au, Sc, Ti, V, Cr, Mn, Fe (dark spheres). The roman numerals identify each geometry in Table I.

-Au distance d_{av} and the geometry of Au_2M^+ isomers can be complemented with another observation relating d_{av} and the multiplicity M_z+1 of first and second isomers: the larger is d_{av}; the larger is the multiplicity. Thus, the multiplicity M_z+1 of the second isomer of Au_2M^+ clusters increases for M=Sc, Ti and decreases for M=V. Instead, for M=Cr, Mn, Fe, whose d_{av} for the first and second isomers differs by less than 0.06 Å, the multiplicity remains unchanged. This empirical relation between geometry, M coordination, average M-Au distance, and multiplicity of Au_2M^+ clusters, is verified also for larger clusters. With a few exceptions, such as Au_8V^+ and Au_8Fe^+, the larger is the average M-Au distance and the smaller the coordination, the larger the multiplicity.

At a given size n, the largest binding energy per atom is obtained for Au_nSc^+, and the lowest is obtained for Au_nCr^+ (except for Au_nMn^+ with n=2, 8, 9). The binding energy of AuM^+ cations is larger than for the pure Au_2^+ dimer, except for M=Cr. The binding energy per atom of Au_nM^+ with $M \neq$ Sc and $n \geqslant 2$ is always smaller than the one for pure Au_{n+1}^+ cations, except for Au_5Ti^+, Au_5Fe^+, and Au_9Ti^+. Notice that there is an isomer of Au_9Ti^+ with practically the same binding energy (~2.36–2.37 eV/atom) and the average M-Au distance (~2.81–2.82 Å) as the pure Au_{10}^+ cation, but with different geometry (9-II instead 9-I) and multiplicity (triplet

TABLE I. Average first-neighbor M-Au distance, d_{av} (Å), and binding energy per atom, E_b (eV) of the few lowest energy isomers of cationic Au_nM^+ clusters for $1 \leqslant n \leqslant 9$ and M=Au, Sc, Ti, V, Cr, Mn, Fe. The geometry notation is that of Fig. 1, except for the obvious 1-I dimer. The integrated difference of electronic charge between majority and minority spin densities, denoted by M_z, is also given in atomic units. M_z is marked in bold for the ground state.

Au				Sc				Ti				V				Cr				Mn				Fe			
geo	M_z	d_{av}	E_b	geo	M_z	d_{av}	E_b	geo	M_z	d_{av}	E_b	geo	M_z	d_{av}	E_b	geo	M_z	d_{av}	E_b	geo	M_z	d_{av}	E_b	geo	M_z	d_{av}	E_b
1-I	1	2.58	1.13	1-I	1	2.47	1.81	1-I	2	2.46	1.28	1-I	3	2.47	1.16	1-I	4	2.49	0.94	1-I	5	2.45	1.15	1-I	4	2.43	1.47
2-III	0	2.65	2.02	2-I	0	2.47	2.14	2-I	1	2.44	1.72	2-III	4	2.70	1.61	2-III	5	2.70	1.60	2-III	4	2.54	1.39	2-III	3	2.55	1.76
				2-III	2	2.66	1.88	2-III	3	2.65	1.71	2-I	2	2.46	1.45	2-II	5	2.71	1.29	2-I	4	2.54	1.33	2-I	3	2.49	1.67
				2-II	2	2.56	1.60	2-II	3	2.57	1.45	2-II	4	2.61	1.43	2-I	5	2.67	1.24	2-II	6	2.54	1.33	2-II	5	2.48	1.60
3-I	1	2.69	2.00	3-I	1	2.65	2.16	3-I	2	2.67	1.97	3-I	3	2.71	1.86	3-I	4	2.71	1.72	3-I	5	2.67	1.74	3-I	4	2.60	1.97
				3-II	1	2.59	2.15	3-II	2	2.58	1.89	3-II	3	2.63	1.68	3-II	4	2.52	1.55	3-II	5	2.63	1.61	3-II	4	2.59	1.89
4-I	0	2.70	2.15	4-I	0	2.66	2.31	4-I	1	2.64	2.10	4-I	4	2.76	1.95	4-I	5	2.75	1.84	4-I	4	2.67	1.86	4-I	3	2.67	2.04
				4-III	0	2.66	2.28	4-III	1	2.64	2.04	4-II	4	2.77	1.91	4-II	5	2.74	1.80	4-IV	4	2.66	1.84	4-II	3	2.64	1.99
				4-V	2	2.67	2.14	4-II	3	2.72	1.98	4-VI	4	2.70	1.83	4-VI	5	2.70	1.80	4-IV	6	2.63	1.84	4-VI	3	2.58	1.92
				4-V	0	2.67	2.08	4-V	3	2.67	1.96	4-V	4	2.68	1.82	4-V	5	2.74	1.79	4-VI	6	2.71	1.72	4-V	3	2.63	1.90
5-V	1	2.69	2.14	5-II	1	2.73	2.33	5-I	2	2.71	2.21	5-I	3	2.71	2.14	5-I	4	2.73	2.02	5-I	5	2.71	2.08	5-I	4	2.66	2.22
				5-I	1	2.72	2.32	5-II	2	2.73	2.19	5-II	3	2.74	2.09	5-II	4	2.76	1.98	5-II	5	2.69	2.01	5-II	4	2.69	2.17
				5-IV	1	2.76	2.30	5-III	2	2.70	2.07	5-III	3	2.70	1.99	5-III	4	2.74	1.90	5-V	5	2.63	1.95	5-V	4	2.59	2.10
				5-VI	1	2.64	2.16	5-VI	2	2.74	2.04	5-VI	3	2.73	1.97	5-VI	4	2.69	1.88	5-VI	5	2.70	1.92	5-VI	4	2.68	2.08
6-II	0	2.72	2.31	6-I	0	2.77	2.40	6-I	1	2.76	2.25	6-II	4	2.76	2.14	6-III	5	2.88	2.06	6-I	4	2.72	2.06	6-II	3	2.73	2.21
				6-IV	0	2.73	2.37	6-II	3	2.72	2.23	6-III	4	2.82	2.14	6-II	5	2.75	2.06	6-III	6	2.81	2.04	6-III	3	2.74	2.19
				6-V	0	2.79	2.36	6-II	1	2.76	2.21	6-I	2	2.72	2.13	6-I	5	2.73	2.01	6-II	4	2.75	2.03	6-I	3	2.69	2.19
				6-II	2	2.74	2.35	6-III	3	2.81	2.19	6-I	4	2.78	2.11					6-III	4	2.74	2.03				
7-IV	1	2.80	2.31	7-I	1	2.81	2.41	7-I	2	2.78	2.30	7-I	3	2.83	2.23	7-I	4	2.83	2.13	7-I	5	2.74	2.15	7-I	4	2.72	2.28
				7-IV	1	2.82	2.35	7-II	2	2.77	2.23	7-II	3	2.76	2.18	7-II	4	2.83	2.10	7-II	5	2.75	2.12	7-II	4	2.71	2.25
								7-III	2	2.66	2.14	7-III	3	2.69	2.11	7-III	4	2.70	2.04								
8-I	0	2.81	2.40	8-II	0	2.80	2.46	8-II	1	2.79	2.35	8-III	2	2.83	2.25	8-III	5	2.88	2.18	8-III	4	2.82	2.17	8-III	3	2.73	2.28
				8-III	0	2.86	2.45	8-III	1	2.82	2.33	8-II	2	2.78	2.24	8-II	3	2.78	2.15	8-II	4	2.76	2.14	8-II	5	2.70	2.26
												8-II	4	2.78	2.17	8-II	5	2.77	2.11					8-II	4	2.75	2.24
9-I	1	2.81	2.36	9-II	1	2.86	2.47	9-II	0	2.80	2.39	9-II	3	2.83	2.31	9-II	4	2.83	2.21	9-II	3	2.82	2.20	9-II	2	2.75	2.30
				9-V	1	2.85	2.44	9-II	2	2.82	2.37	9-VII	3	2.84	2.29	9-VII	4	2.86	2.20	9-II	5	2.83	2.17	9-II	4	2.76	2.29
				9-VI	1	2.91	2.44	9-III	2	2.78	2.18	9-III	3	2.84	2.18	9-III	4	2.85	2.14	9-IV	5	2.75	2.13	9-IV	4	2.73	2.23
				9-VIII	1	2.89	2.43					9-III	4	2.84	2.16	9-III	6	2.81	2.13	9.III	7	2.78	2.10	9-III	4	2.72	2.21

instead singlet). A similar situation is found for the isomer Au_5Fe^+ with 5-II geometry and $M_z=4$. Thus, substituting an Au atom by a M atom is always energetically unfavorable for Au_nM^+ clusters ($2 \leqslant n \leqslant 9$) except for M=Sc, and for Au_5Ti^+, Au_5Fe^+, and Au_9Ti^+.

Trends in the binding energies are clearly seen in Fig. 2 for clusters with $3 \leqslant n \leqslant 8$. We observe that the curves for $n=5$ and $n=7$ depart from the pattern shown by the curves with other constant n values. As a consequence, the shift between curves $n=5$ and $n=4$ decreases for Sc and increases for the other impurities, whereas the reverse happens for the shift between curves $n=5$ and $n=6$. This fact allows our calculations to explain the enhanced relative abundance observed for Au_6Sc^+, on one hand, and for Au_5M^+ with $M \neq$ Sc, on the other hand.

We see in Fig. 2 that the curve $n=6$ widens (narrows) the shift with the curve $n=5$ ($n=7$) for Sc whereas the contrary occurs for the remaining impurities. For Ti the curve $n=6$ is halfway between the $n=5$ and $n=7$ binding energy curves. This behavior, which is a consequence of the tendency of curves $n=5$ and $n=7$ commented on previously, leads to the special stability of doped Au_nM^+ cations at $n=6$ for Sc, $n=5$ for Ti, and $n=5,7$ for the other M impurities, in perfect agreement with experimental abundances of photofragmented Au_nM^+ clusters.[2]

The extra stability observed[2] at certain sizes (magic numbers) of Au_nM^+ clusters can be related to peaks of the second total energy difference, defined by Eq. (3). In the left panels of Fig. 3 we represent the calculated Δ_2E_n for Au_nM^+ clusters. The experimental abundance peaks at $n=6$ for M=Sc,

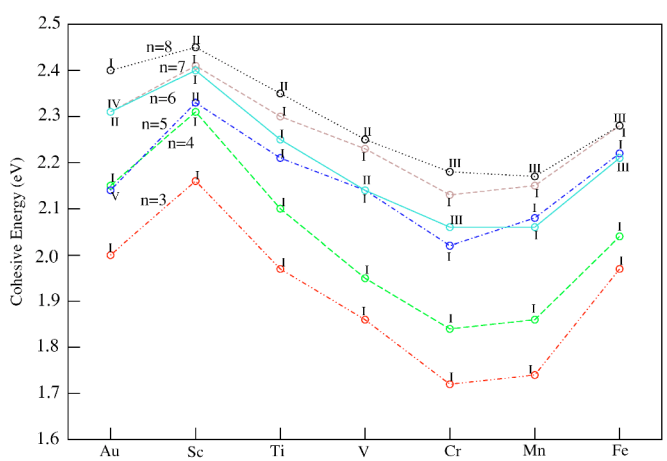

FIG. 2. (Color online) Binding energy per atom for Au_nM^+ clusters with $3 \leqslant n \leqslant 8$. The Roman numerals indicate the geometry label of Table I and Fig. 1. The data points are connected for a given n only to guide the eye.

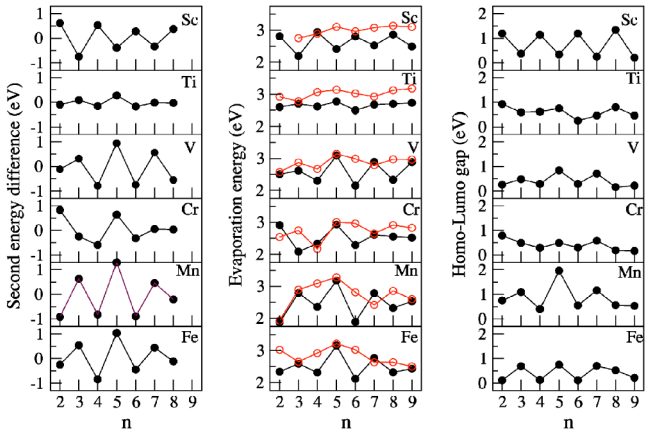

FIG. 3. (Color online) Left panels: Second total energy differences, Eq. (3), versus number of gold atoms for Au_nM^+ clusters. Middle panels: Evaporation energy of a neutral Au atom (filled dots) and of a dimer Au_2 (empty dots). For Sc the dimer evaporation energy is 3.90 eV. Rights panels: HOMO-LUMO gap of the ground state.

$n=5$ for $M=$Ti, and $n=5,7$ for $M\neq$Sc, Ti, coincide also with the pattern seen in Δ_2E_n. Notice that the positive-negative alternation of Δ_2E_n values calculated using Eq. (3), is in agreement with the alternation of positive-negative values of $\ln(I_n/I_{n+1})$ calculated from observed abundances I_n. This fact should be expected, according to Eqs. (1)–(3), assuming a good total energy calculation.

In the middle panels of Fig. 3 are given the evaporation energies of a neutral Au atom and of a Au_2 dimer. Except in a few cases, barriers for atomic Au evaporation, E_{ev}, are lower than for losses of Au_2. $E_{ev}(n)$ shows positive peaks at the same number n of Au atoms as Δ_2E_n. In the right panels of Fig. 3 we present the difference between the eigenvalues of the lowest unoccupied molecular orbital (LUMO) and the highest occupied molecular orbital (HOMO), known as the HOMO-LUMO gap. It is currently believed that the higher is this gap the higher is the cluster stability relative to the neighbors' sizes. Thus, peaks in the HOMO-LUMO gap appear at the same n values already commented on for Δ_2E_n and for $E_{ev}(n)$.

The results in Figs. 1–3 are obtained from first principles calculations and cannot be reinterpreted in terms of the spherical shell model of quasi-free electrons. As noted in Sec. I, in order to explain the experimental abundances[2] within that simple model, one needs to assume that the 3*d* electrons of the *M* impurity are completely delocalized in Sc and Ti, and completely localized in the remaining 3*d* *M* series.

B. Impurity charge and local magnetic moment

We have performed a Mulliken charge population analysis in order to study the localization of the positive charge in the Au_nM^+ cations. The results for $n=1$, 5 are collected in Table II, and the results for $1\leqslant n\leqslant 9$ and $M=$Sc, Ti, are collected in Table III. Contrary to the covalent situation for pure gold cations, where the less coordinated atoms have the larger positive charge, for $M\neq$Au the charge is localized mostly at the impurity, with a decreasing value when the cluster size increases. This is because the coordination with Au atoms increases. For the smaller cluster sizes, the Au-*M* bond is mainly ionic, and the amount of charge transfer to Au atoms follows roughly the sequence of electronegativity difference between Au and *M* atoms. For $n=5$ the *M* coordination to Au atoms is much more higher and the charge at the *M* atom becomes stabilized around a value $\sim$0.5–0.6. Our results in Tables II and III agree qualitatively with the results of Janssens and co-workers[3] obtained with natural population analysis.

The magnetic moment of the impurity as a function of the cluster size, shows pronounced odd-even effects. For example, for Au_nSc^+ and Au_nTi^+ we obtain the results collected in Table III. This can be correlated to the odd-even trend in th M_z values of the clusters in Table I already commented on in Sec. III A. For Au_nSc^+ clusters with odd *n*, the magnetic moment of the impurity decrease drastically when *n* increases from 1 to 9, whereas for even *n* values, the magnetic moment of Sc is zero, in correspondence with the M_z values

TABLE II. Positive charge, *q* (in a.u.), and local magnetic moment, μ (in μ_B), on the *M* atom of Au_nM^+ clusters with $n=1,5$ obtained from the Mulliken population analysis. The last four rows list calculated μ values of the *M* impurity adsorbed on different Au surfaces (Refs. 22 and 23) and embedded in Au bulk (Ref. 21). These values are extracted from figures in several publications (Refs. 23, 22, and 21).

M	Au	Sc	Ti	V	Cr	Mn	Fe
$q(AuM^+)$	0.50	0.97	0.88	0.83	0.80	0.81	0.76
$q(Au_5M^+)$	0.16	0.59	0.52	0.50	0.51	0.55	0.51
$\mu(AuM^+)$	0.50	1.07	2.16	3.29	4.62	5.12	4.00
$\mu(Au_5M^+)$	0.22	0.40	1.87	3.10	4.25	4.95	3.82
μ M/(001)[a]			1.80	3.10	4.20	4.50	3.20
μ M/(110)[b]			0.90	2.45	3.60	4.25	3.10
μ M/(111)[b]			0.00	2.50	3.80	4.30	3.30
μ M/bulk[c]				2.40	3.60	4.00	3.00

[a]Reference 23
[b]Reference 22
[c]Reference 21

TABLE III. Positive charge, q (in a.u.), and local magnetic moment, μ (in μ_B), on the M atom of Au_nM^+ clusters with $1 \leqslant n \leqslant 9$ and M=Sc, Ti obtained from Mulliken population analysis. * There exist the isomeric state 9-II triplet with q=0.33, and μ=1.24.

	1	2	3	4	5	6	7	8	9
$q(Au_nSc^+)$	0.97	0.87	0.75	0.63	0.59	0.47	0.45	0.39	0.35
$q(Au_nTi^+)$	0.86	0.73	0.67	0.53	0.52	0.41	0.41	0.37	0.30*
$\mu(Au_nSc^+)$	1.07	0.00	0.62	0.00	0.40	0.00	0.28	0.00	0.13
$\mu(Au_nTi^+)$	2.18	1.29	1.92	1.25	1.87	1.25	1.62	1.25	0.00*

reported in Table I. For Au_nTi^+ clusters, the M magnetic moment remains practically constant for even $n \geqslant 4$ values, and decreases regularly for odd n values, droping drastically to zero for n=9. Notice that for the isomeric state 9-II of Au_9Ti^+, with M_z=2, the magnetic moment is $1.24\mu_B$, close to the value $1.25\mu_B$ of the neighbor cluster Au_8Ti^+. We have already observed that isomers of Au_9Ti^+ have a similar binding energy and average M-Au distance to the pure Au_{10}^+ cation. It is interesting to note that in a recent DFT calculation by Fan and Gong[22] it is obtained that the magnetic moment of a Ti atom adsorbed on the Au (111) surface is zero, but it is $\sim 0.9\mu_B$ when Ti is adsorbed on the Au (110)-(1×2) surface. In another calculation,[23] the magnetic moment of Ti is $\sim 1.80\mu_B$ when adsorbed on the Au (001) surface. This result, quoted also in Table I, shows that the magnetic moment is very sensitive to the geometrical environment. In the case of our two isomers Au_9Ti^+ with geometry 9-II, the difference in the spin multiplicity and the Ti magnetic moment is due to the different average M-Au bond distance. There are other clusters, like Au_9Mn^+ and Au_9Fe^+, with isomeric states whose binding energy and average M-Au distance are close to the ground state ones, but with M_z values two units larger.

In Table II are also given, for comparison, the calculated magnetic moment of the M impurity adsorbed on the Au surfaces (001) (Ref. 23), (110)-(1×2) (Ref. 22), (111) (Ref. 22), and embedded in Au bulk.[21] In these works the orbital contribution to the magnetic moment is also calculated, but is not taken into account here. For pure transition metal clusters M_n of the magnetic elements (M=Fe, Co, Ni) with $n \leqslant 10$, it was estimated[24] that the orbital magnetism contributes more than 20% to the total cluster magnetization. However, in a recent work[22] the orbital contribution to the magnetic moment of a transition metal atom adsorbed on different gold surfaces was estimated to be $\leqslant 0.1\mu_B$ for the M elements considered in this work. Notice that the environment of the transition metal atom in our Au_nM^+ clusters resembles the one of a planar surface, instead of the environment of a M atom in bulk gold. As discussed by Guirado-Lopez and co-workers,[24] kinetic energy enhancement, which favors electron delocalization, acts contrary to Coulomb interactions, which tend to suppress charge fluctuations and lead to Hund rules, with enhanced (but different energy scale) orbital and spin moments. The interpretation of the abundance experiments of Au_nM^+ clusters by Neukermans and co-workers[2] as due to the delocalized behavior of the d electrons of the M impurity, supports the fact that the orbital moment of M is small. We see in Table II that the magnetic moments of Au_5M^+ clusters are close to those of the M impurity on the (001) surface of Au. Nevertheless, the comparison of the magnetic moment calculated for the M atom adsorbed on different gold systems, as proposed in Table II, should be taken with caution, due to both the different type of calculation and the different environment of the impurity.

IV. CONCLUSIONS

Using first-principles total energy calculations we have calculated the atomic and electronic structure of a few lowest energy isomers of gold cluster cations doped with a 3d M atom, Au_nM^+. For the lowest energy isomer of clusters with $n \leqslant 6$ we obtain planar geometries, which are practically degenarate with a 3D structure in the case of Au_6V^+ and Au_6Cr^+.

We obtain empirical qualitative relations between geometry, M coordination, average M-Au distance, and multiplicity of Au_2M^+ clusters, which are verified also for larger clusters. With a few exceptions, the larger is the average M-Au distance and the smaller the coordination, the larger is the multiplicity. An additional example to the ones already commented on in Sec. III A is Au_6Cr^+, with a 3D isomeric state having an 0.02 eV/atom larger binding energy, and the same coordination number for Cr than the planar 6-I lowest energy state, but a 0.09 larger d_{av} distance and 2 units larger M_z value.

We obtain the observed magic numbers for Au_nM^+ clusters[2] without resorting to the empirical shell model of delocalized electrons. Trends versus n of the binding energies, HOMO-LUMO gap, second differences of total energies, and monomer evaporation energies show these magic numbers clearly, namely, n=6 for Sc, n=5 for Ti, and n=5,7 for V, Cr, Mn, Fe.

The positive charge of the cationic Au_nM^+ clusters is localized mainly in the impurity and decreases when the size of the cluster increases.

The magnetic moment of the impurity as a function of the cluster size shows pronounced odd-even effects, and is very sensitive to the geometrical environment and to the average M-Au distance.

ACKNOWLEDGMENTS

We appreciate the support of the Junta de Castilla y León (Grants No. VA073/02 and No. VA060/03), and from MCyT (Grant No. MAT2002-04393-C02-01). EMF acknowledges a FPU grant from the Ministerio de Educacion y Ciencia of Spain.

*E-mail address: begonia@ubu.es
†E-mail address: eva@lcb.fam.cie.uva.es
‡E-mail address: balbas@lcb.fam.cie.uva.es

[1] K. Palotás, B. Lazarovits, L. Szunyogh, and P. Weinberger, Phys. Rev. B **70**, 134421 (2004).
[2] S. Neukermans, E. Janssens, H. Tanaka, R. E. Silverans, and P. Lievens, Phys. Rev. Lett. **90**, 033401 (2003).
[3] E. Janssens, H. Tanaka, S. Neukermans, R. E. Silverans, and P. Lievens, Phys. Rev. B **69**, 085402 (2004).
[4] X. Li, B. Kiran, J. Li, H.-J. Zhai, and L.-S. Wang, Angew. Chem., Int. Ed. **41**, 4786 (2002).
[5] W. Bouwen, F. Vanhoutte, F. Despa, S. Bouckaert, S. Neukermans, L. T. Kuhn, H. Weidele, P. Lievens, and R. E. Silverans, Chem. Phys. Lett. **314**, 227 (1999).
[6] M. Heinebrodt, N. Malinowski, F. Tast, W. Branz, and T. P. Martin, J. Chem. Phys. **110**, 9915 (1999).
[7] E. Janssens, H. Tanaka, S. Neukermans, R. E. Silverans, and P. Lievens, New J. Phys. **5**, 46 (2003).
[8] H. Tanaka, S. Neukermans, E. Janssens, R. E. Silverans, and P. Lievens, J. Am. Chem. Soc. **125**, 2862 (2003).
[9] H. Tanaka, S. Neukermans, E. Janssens, R. E. Silverans, and P. Lievens, J. Chem. Phys. **119**, 7115 (2003).
[10] B. R. Sahu, G. Maofa, and L. Kleinman, Phys. Rev. B **67**, 115420 (2003).
[11] P. Pyykkö and N. Runeberg, Angew. Chem., Int. Ed. **41**, 2174 (2002).
[12] C. E. Klots, J. Chem. Phys. **92**, 5864 (1988).
[13] J. M. Soler, E. Artacho, J. D. Gale, A. García, J. Junquera, P. Ordejón, and D. S. Portal, J. Phys.: Condens. Matter **14**, 2745 (2002).
[14] W. Kohn and L. J. Sham, Phys. Rev. **145**, 561 (1965).
[15] J. P. Perdew, K. Burke, and M. Ernzerhof, Phys. Rev. Lett. **77**, 3865 (1996).
[16] N. Troullier and J. L. Martíns, Phys. Rev. B **43**, 1993 (1991).
[17] L. Kleinman and D. M. Bylander, Phys. Rev. Lett. **48**, 1425 (1982).
[18] E. M. Fernández, J. M. Soler, I. L. Garzón, and L. C. Balbás, Phys. Rev. B **70**, 165403 (2004).
[19] E. M. Fernández, M. B. Torres, and L. C. Balbás, Int. J. Quantum Chem. **99**, 39 (2004).
[20] L. C. Balbás, J. L. Martíns, and J. M. Soler, Phys. Rev. B **64**, 165110 (2001).
[21] S. Frota-Pessôa, Phys. Rev. B **69**, 104401 (2004).
[22] W. Fan and X. G. Gong, cond-mat/0407746 v2.
[23] I. Cabria, B. Nonas, R. Zeller, and P. H. Dederich, Phys. Rev. B **65**, 054414 (2002).
[24] R. A. Guirado-López, J. Dorantes-Dávila, and G. M. Pastor, Phys. Rev. Lett. **90**, 226402 (2003).